Proceedings of the International Heat Transfer Conference
IHTC14
August 8-13, 2010, Washington, DC, USA

IHTC14-22520

FLOW AND THERMAL FIELDS IN A PENDANT DROPLET MOVING ON LYOPHOBIC SURFACE

Basant Singh Sikarwar
Department of Mechanical Engineering
Indian Institute of Technology Kanpur
Kanpur 208016, India
sikarwar@iitk.ac.in

K. Muralidhar
Department of Mechanical Engineering
Indian Institute of Technology Kanpur
Kanpur 208016, India
kmurli@iitk.ac

Sameer Khandekar
Department of Mechanical Engineering
Indian Institute of Technology Kanpur
Kanpur 208016, India
samkhan@iitk.ac.in

ABSTRACT

Clusters of liquid drops growing and moving on physically or chemically textured lyophobic surfaces are encountered in drop-wise mode of vapor condensation. As opposed to film-wise condensation, drops permit a large heat transfer coefficient and are hence attractive. However, the temporal sustainability of drop formation on a surface is a challenging task, primarily because the sliding drops eventually leach away the lyophobicity promoter layer. Assuming that there is no chemical reaction between the promoter and the condensing liquid, the wall shear stress (viscous resistance) is the prime parameter for controlling physical leaching. The dynamic shape of individual droplets, as they form and roll/slide on such surfaces, determines the effective shear interaction at the wall. Given a shear stress distribution of an individual droplet, the net effect of droplet ensemble can be determined using the time averaged population density during condensation.

In this paper, we solve the Navier-Stokes and the energy equation in three-dimensions on an unstructured tetrahedral grid representing the computational domain corresponding to an isolated pendant droplet sliding on a lyophobic substrate. We correlate the droplet Reynolds number (Re = 10-500, based on droplet hydraulic diameter), contact angle and shape of droplet with wall shear stress and heat transfer coefficient. The simulations presented here are for Prandtl Number (Pr) = 5.8. We see that, both Poiseuille number (Po) and Nusselt number (Nu), increase with increasing the droplet Reynolds number. The maximum shear stress as well as heat transfer occurs at the droplet corners. For a given droplet volume, increasing contact angle decreases the transport coefficients.

INTRODUCTION

The sliding of liquid drops underneath a lyophbic surface has been a subject of extensive research in many industrial and engineering applications such as drop-wise condensation heat transfer, microfluidics, lab-on-chip device, ink jet printing systems, spraying of insecticide on crops and several biochemical processes. It is know that the dynamic steady state of condensing vapors on a cold substrate involves a large population or ensemble of droplets, representing various temporal generations [1-4]. The droplets increase in size by combination of direct condensation and coalescence with neighboring droplets [5-6]. As droplets grow, the body forces eventually exceed the droplet retention force due to surface tension which leads to sliding of drops and eventual fall off. This exposes virgin substrate portions where another temporal generation of droplets begins to grow; the cycle is repeated as shown in Figure 1.

The long term sustainability of dropwise condensation depends on the shear interaction of sliding droplets with the promoter layer creating lyophobicity. The phenomenon of removal of promoter layers or surface damage due to sliding of drop is called surface leaching. This phenomenon is primarily affected by viscous forces at the contact surface, chemical reactions between the condensing liquid and the lyophobic promoter; the heat transfer rate and temperature fluctuations will also affect these interactions. Open literature on surface leaching due to droplet motion is limited. Most of the existing works [7-13] have considered static critical state of sessile drop on inclined surface and focused on the contact angle hysteresis, drop shape, and drop retention with tiltable surface of various combinations

of the hydrophobic surface and the liquid. Elsherbine and Jacobi [12-13] performed experiments on an isolated sessile droplet and reported that the drop is deformed at the static critical state of an inclined plane. They investigated the geometric parameters necessary to describe the shape of the sessile drop and retention forces at this state.

Though a large volume of work exists on the drop shape, its spreading and stability on a tilted plane, very few researchers have reported the sliding behavior of the drop on inclined surface [14-26]. Kim et al. [14] performed experiments for measuring the steady sliding velocity of different liquid drops on an inclined surface and reported a scaling law to determine the sliding velocity of a liquid droplet of known wetting characteristics. Huang et al. [15] used a numerical technique, i.e. the front tracking method, to determine the motion of two-dimensional drops and bubbles on a partially wetting surface exposed to shear flow. Gao and McCarthy [16] postulated two mechanisms for drop moving down the plane. Droplets can move by sliding where the particles near the solid-liquid interface exchange their position with those at the gas-liquid interface while the bulk of the fluid remains unaffected. The particle movement along the gas- liquid and solid-liquid interfaces is similar to the motion of a tread of a chain-driven tank. On the other hand, there could be rolling motion where the entire fluid mass undergoes a circulatory movement. Suzuki et al. [17] studied the sliding behavior of water droplets on various chemically textured surfaces at a fixed inclination of 35^{o} and reported the sliding displacement of the advancing edge of the droplet. Sakai et al. [18] studied the rolling versus sliding behavior of droplet on various chemically textured surfaces. Annapragada et al. [19] have performed experiments to characterize the velocity dependence of advancing and receding angles as a function of the Capillary number. In their theoretical analysis, Grand et al. [20] scaled the viscous force as $\mu UV^{1/3}$ and reported that the drop sliding velocity along an inclined plane is a linear function of the Bond number. Yoshida et al. [21] did not consider the viscous force in their study of sliding behavior of water droplets on a flat polymer surface. The authors reported that the sliding motion changes from constant velocity to one of constant acceleration with an increase in the contact angle. Daniel et al. [22] reported the maximum velocity of the condensing sessile drop on a chemically textured surface. Sakai and Hashimoto [23] have experimentally determined the velocity vector distribution inside a sliding sessile drop using PIV. The authors reported that the velocity gradient near the liquid-solid interface is higher than locations elsewhere inside a drop. This analysis was further used to recognize the slipping and rolling components of the sliding velocity and the acceleration of the water droplet [24]. Das and Das [25] used smooth particle hydrodynamics (SPH) to numerically simulate the movement of drops down an inclined plane. The study captured the internal circulation inside a sliding sessile drop. It was shown that the frictional resistance by viscosity at the interface of solid and liquid cannot be neglected in estimating the sliding behavior and related effects for a droplet moving on an incline substrate.

To the best of the knowledge of the authors there is no literature available that correlates droplet shape and flow parameters with wall shear stress (friction coefficient) and heat transfer coefficient (Nusselt Number) of an isolated droplet sliding underneath a lyophobic surface. We have therefore aimed at providing a correlation between the droplet shape, contact angle, volume, sliding velocity and the ensuing friction factor as well as the heat transfer coefficient. Section 2 of the paper describes the mathematical formulation of the problem and defines of the non-dimensional numbers of interest. Sections 3 and 4 describe the procedures of calculation of wall shear stress and wall heat transfer coefficient and discuss the implications thereof. Finally, conclusions are reported in Section 5.

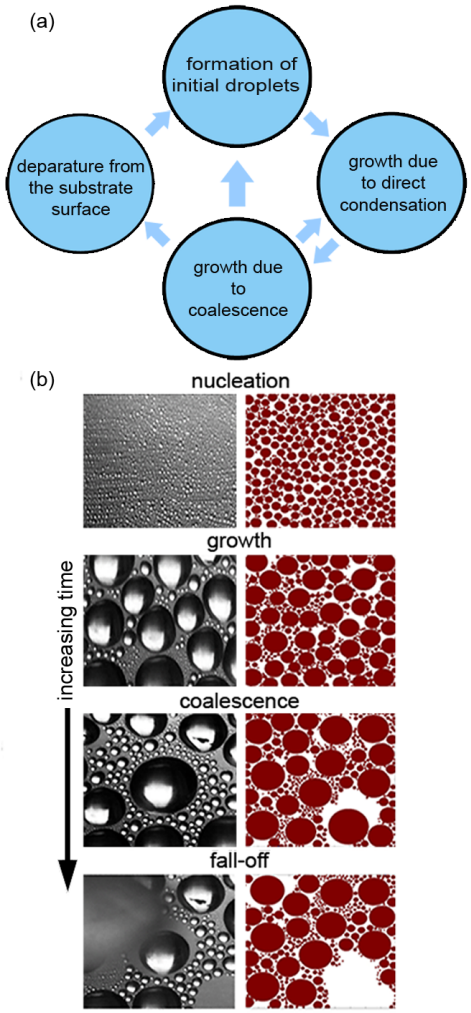

Figure 1: Complete cycle of dropwise condensation underneath chemically textured inclined surface [5]. (a) Cycle of drop formation to sliding motion and finally a gravitational falloff. (b) Experimentally observed cycle and cycle captured by computer simulation.

NOMENCLATURE

$A_{yz\|max}$	maximum cross-sectional area of the droplet in the YZ plane (m^2)
C_p	specific heat of the liquid (J/kg-K)
D_{hyd}	hydraulic the diameter of the droplet (m)
d	diameter of the droplet (m)
d_b	base diameter of the droplet (m)
H	maximum height of the droplet (m)
h	heat transfer coefficient (W/m^2-K)
k	thermal conductivity (W/m-K)
$\overline{n}$	unit normal vector of the surface (-)
P	wetted perimeter, length of the contact line (m)
p	pressure (Pa)
q	heat flux (W/m^2)
t	time (s)
$\overline{t}$	unit tangent vector (-)
T	temperature (ºC)
ΔT	temperature difference between wall and the drop interface (ºC)
u	velocity (m/s)
U_{wall}	sliding velocity of the wall (m/s)
V	volume of drop (m^3)
ρ	density (kg/m^3)
μ	dynamic viscosity (Pa-s)
σ	surface tension (N/m)
ϕ	viscous dissipation function ($1/s^2$)
τ	shear stress (N/m^2)
τ_{wall}	wall shear stress (N/m^2)
θ	contact angle (°)
θ_a	advancing angle of the droplet (°)
θ_r	receding angle of the droplet (°)

Non-dimensional parameters

Bo	Bond number $(\rho g d_b^2 / \sigma)$
Ca	Capillary number $(\mu U_{wall} / \sigma)$
C_f	Coefficient of friction $(\tau_{wall} / \rho U^2_{wall})$
Nu	Nusselt number $(h d_b / k)$
Po	Poiseuille number $(C_f \cdot Re)$
Pr	Prandtl number $(\mu C_p / k)$
Re	Reynolds number $(\rho U_{wall} D_h / \mu)$

Subscripts

a	advancing angle
b	base of the droplet
f	friction
free	free surface of the droplet
hyd	hydraulic
i	free indices
j	repeated indices
max	maximum
p	pressure
r	component in radial direction; spherical coordinates
wall	wall
x, y, z	component in the *x, y,* or *z* direction respectively
xy	*xy* plane
yz	*yz* plane
zy	*zy* plane
θ	component in the θ direction, spherical coordinates
ϕ	component in the ϕ direction, spherical coordinates

MATHEMATICAL DESCRIPTION

The schematic diagram of the three-dimensional deformed drop with an advancing angle 105° and a receding angle 55° as well as symmetric drops of various contact angles (90, 105 and 120°) are shown in Figure 2. The liquid droplet is treated as fixed relative to which the wall (substrate) is moving at a constant speed. The volume of the droplet for all computations is fixed and is equal to 134 µl. The shape of drops for various contact angles is taken to be a part of sphere while the shape of the deformed droplet is determined by a procedure described by Sikarwar et al. [6][1].

The hydraulic diameter of the droplet is calculated with respect to the maximum cross section of drop over the YZ plane ($A_{yz|\max}$) and the wetted perimeter, P, of the droplet base area on the wall (substrate), as given below (refer Fig. 3):

$$D_{hyd} = \left(4 \cdot A_{yz|\max}\right) / P \qquad (1)$$

Wall shear stress is determined by solving the three dimensional Navier-Stokes equation; the boundary conditions are no slip at the wall and free surface (zero shear) elsewhere on the droplet. The wall heat transfer coefficient is obtained by solving the three dimension energy equation for a pair of constant temperature boundaries at the wall and the free surface respectively, as given by Eqs. (2-5). Boundary condition at the free surface is in spherical coordinates as given by Eq. (5). They need to be transformed from spherical to Cartesian coordinates during the numerical implementation. For a deformed drop, a local coordinate system is used for boundary conditions. The flow field and heat transfer rates have been obtained for Reynolds numbers in the range 10-500 at Pr = 5.8.

The governing equations for an incompressible liquid with proper boundary conditions are summarized as follows:

$$\rho\left(\frac{\partial u_i}{\partial t} + u_j \frac{\partial u_i}{\partial x_j}\right) = -\frac{\partial p}{\partial x_i} + \mu \frac{\partial^2 u_i}{\partial x_j^2} \qquad (2)$$

$$\rho \cdot C_p\left(\frac{\partial T}{\partial t} + u_j \frac{\partial T}{\partial x_j}\right) = k \frac{\partial^2 T}{\partial x_j^2} + \mu \cdot \phi \qquad (3)^2$$

[1] The shape of liquid-vapor interface is obtained by solving the Young-Laplace equation that enforces a balance between pressure force, gravity and surface tension. Static equilibrium condition leads to the rate of change of curvature at each location of the droplet, which is solved by the Runge-Kutta method. The details are given in [6].

[2] The contribution of viscous dissipation was found to be insignificant.

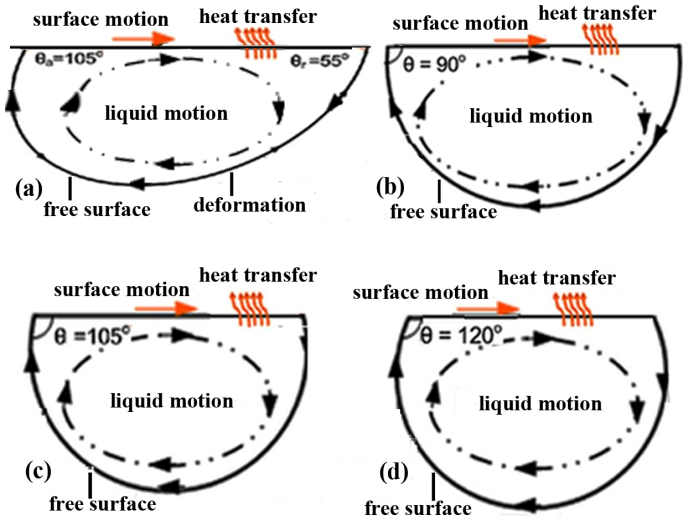

Figure 2: Schematic diagram of (a) a deformed drop (b) a symmetric drop with contact angle 90°, (c) a symmetric drop of contact angle 105°, and (d) a symmetric drop of contact angle 120°.

Boundary condition at the wall and the free surface:

$$u_x = U_{wall};\ u_y = 0;\ u_z = 0;\ T = T_{wall} \tag{4}$$

$$u_r = 0;\ \tau_{r\theta} = 0;\ \tau_{r\phi} = 0;\ T = T_{free} \tag{5}$$

Fluid flow and heat transfer rates inside the drop have been obtained by numerically solving the unsteady Navier-Stokes and energy equations in three dimensions. The drop deformation arising from fluid motion is neglected. From the flow and temperature distributions, the wall shear stress and heat transfer coefficient are calculated from Eq. (6) followed by Eqs. (7-8).

$$\left.\begin{aligned} \tau_{xy} &= \mu\left[\left(\partial u_x/\partial y\right)+\left(\partial u_y/\partial x\right)\right]_{wall} \\ \tau_{zy} &= \mu\left[\left(\partial u_z/\partial y\right)+\left(\partial u_y/\partial z\right)\right]_{wall} \\ \tau_{wall} &= \sqrt{\tau_{xy}^2+\tau_{zy}^2} \end{aligned}\right] \tag{6}$$

$$q = -k\left[\frac{\partial T}{\partial n}\right] = -k\left[\frac{\partial T}{\partial y}\right]_{wall} \tag{7}$$

$$h = q/\Delta T \tag{8}$$

Here, ΔT is the temperature difference between the wall and the surface of the droplet.

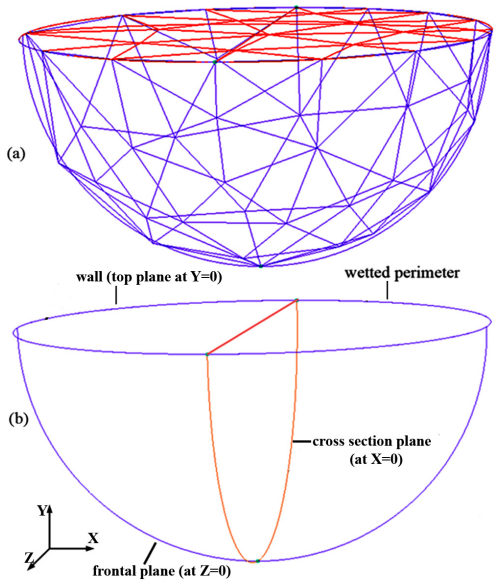

Figure 3: Computational domain within the drop. (a) Triangular base of the tetrahedral element is shown on the surface. (b) Various planes of the drop of contact angle 90°.

The Reynolds number is defined on the basis of the hydraulic diameter of the drop and Prandtl number is defined at an average temperature (mean temperature of the two boundary conditions) of the drop.

$$\text{Reynolds number (Re)} = \left(\rho \cdot U_{wall} \cdot D_{hyd}\right)/\mu \tag{9}$$

$$\text{Prandtl Number (Pr)} = \left(\mu \cdot C_p\right)/k \tag{10}$$

$$\text{Nusselt Number (Nu)} = \left(h \cdot D_{hyd}\right)/k \tag{11}$$

NUMERICAL METHODLOGY

The computational approach adopted in the present study is based on finite volume discretization (FVM) of the three dimensional unsteady Navier-Stokes and energy equations over an unstructured mesh. Between vertex-centered and cell-centered placement of variables, the pressure correction procedure is cell centered, collocated with the fluid velocities [26]. The unstructured mesh is filled with tetrahedral elements of nearly equal volumes. Pressure-velocity coupling is treated using a smoothing pressure correction method that results in a SIMPLE-like algorithm. Convective terms are discretized by a second order upwind scheme. Geometry invariant features of the tetrahedral element are used so that the calculation of gradients at cell faces is simplified using nodal quantities of a particular variable. Nodal quantities, in turn, are calculated as a weighted average of the surrounding cell-centered values [27]. The diffusion terms are discretized using a 2nd order central-difference scheme.

Free surface boundary is discretized in spherical coordinates and transformed to Cartesian coordinates. The discretized free

surface boundary condition is described in the previous work of the authors [6]. The discretized system of algebraic equations is solved by the Stabilized Bi-Conjugate Gradient method (biCGStab) with a diagonal pre-conditioner. The overall solution algorithm used for the present study is quite similar to that proposed by Date [28]. Points of difference are related to the use of certain invariant properties of the tetrahedral element, powerful linear equations solver as well as a parallel implementation of the computer program. Iterations within the code are run till a convergence in terms of the absolute residual of order $\sim 10^{-7}$ is reached.

The computer code has been validated against many benchmark problems, such as, a three-dimensional lid driven cavity at Re = 400 [29], as shown in Figure 4, flow through pipe and experimental results of steady flow through the human carotid bifurcation available [30]. Close agreements lend the desired validation of the code. The number of cells within the drop required for grid independence at the highest Reynolds number was close to 700,000.

RESULTS AND DISCUSSION

To give a complete picture of the flow patterns inside a sliding drop, computed predictions are displayed in the form of velocity profiles, contours of velocity magnitude, velocity vectors, streamline plots, wall shear stress, dimensionless temperature, wall heat transfer coefficient as well as wall pressure distribution. Reynolds numbers considered are Re = 10, 50, 100, and 500 at a Prandtl number of 5.8. A typical computational domain with triangular faces on the boundary, tetrahedral elements inside the droplet volume and the corresponding Cartesian coordinate system is shown in Figure 3(a) for a contact angle of 90°. Similar grids are generated for other geometries – symmetric and deformed. Flow parameters are displayed on the X-Y plane (frontal plane) where Z=0, X-Z plane where Y=0 and Z-Y plane (cross section plane) where X=0 as shown in Figure 3(b). The fluid flow patterns inside the drop of contact angle 90°, 105°, and 120° respectively are shown in Figures 5-12. The velocity vectors and the velocity profile at the center of the frontal plane (corresponding to $A_{xy|max}$, at X=0) have been shown in Figures 5-7. The results show that the *u* velocity variation is nearly linear with respect to height (*y*) of the drop at X=0. These results are in agreement with the PIV studies reported in [18] and [24]. With increasing Re, the location inside the drop where the *x*-component velocity changes its sign shifts towards the base of the drop. In this plane, the magnitude of velocity at the free surface nearly matches the imposed wall velocity though in the opposite direction. Qualitatively comparing drops of contact angles 90°, 105°, and 120° respectively, we find that there is no major difference in the distributions of velocity components and therefore the overall flow pattern. Deformed drops also show similar qualitative flow distribution at various Reynolds numbers. The point of zero velocity was seen to move closer to the solid wall at Reynolds numbers of 1000 and higher. On the Y-Z plane, multiple cells of circulations were observed creating a low pressure zone across the drop (Figures 8-9). The velocity vectors in Figures 5-7 agree well with published experimental data [25] and the smooth particle hydrodynamics estimations in [26].

The derived flow parameters (wall pressure and wall shear stress) for symmetric drops at various contact angles are shown in Figures 8-13. The pressure distributions at the wall surface are shown in Figures 8-10. The pressure distributions at the wall are seen to be qualitatively similar in these cases. It is seen that the wall pressure at the center of the base is smaller (negative) than that towards the sides. Figures 8-10 also show that wall pressure variation is heightened for increasing values of Reynolds number. The wall shear stress distribution, determined by using Eq. (6), for Reynolds number 10 to 500 are shown in Figures 11-13. It is understandable that the region close to the contact line is a high shear zone [31, 32]. This is clearly seen in Figures 11-13, as we move away from the contact line and come in the inner zone of the base of the drop, the shear stress reduces. It can also be clearly observed that average shear stress is a strong function of the Reynolds number. It is also dependent on the contact angle. This is quantitatively depicted in Fig. 13 for the average wall shear stress which highlights increase in the Poiseuille number with increase in Reynolds number. The average wall shear stress distribution is high for a deformed drop in comparison to symmetric drop of contact angles 90°, 105° and 120° respectively, as shown in Figure 13.

The non-dimensional temperature $= \left(T - T_{wall}\right) / \left(T - T_{free}\right)$ contours inside the drop on selected frontal planes are shown in Figures 15-17. Near the wall and the free surface, the normal velocity component is zero and diffusion is the dominant mode of heat transfer. At low Re, on the line of symmetry on the XY plane, temperature decreases monotonically from the free surface to the wall. In contrast, we see a shift in this monotonic trend at higher Reynolds numbers (> 100). Owing to strong circulation and three dimensionality in the flow in the cross-sectional plane X=0 (YZ), there occurs a temperature inversion at the core of the drop, as one moves from the substrate to the free surface (Figure 18(a)). The related temperature distribution is shown in Figure 18(b). At high Re, the flow was seen to be unsteady as well.

Figures 19-21 show the local heat transfer coefficient at the wall for various Reynolds numbers in terms of the Nusselt number. The heat transfer rate increases as Reynolds number increases due to stronger mixing. The heat transfer coefficient at the wall is approximately uniformly distributed at the Reynolds numbers considered, except very near the drop periphery. For each contact angle, Figure 22 shows that the Nusselt number is a nearly a linear function of Reynolds number; slight change of slope, i.e. decrease of Nu is observed around Re ~ 50-100, which, as stated above, is attributed to the temperature inversion phenomena leading to reduced thermal transport. In addition, Nusselt number is large for a contact angle of 90^o and decreases as the contact angle increases.

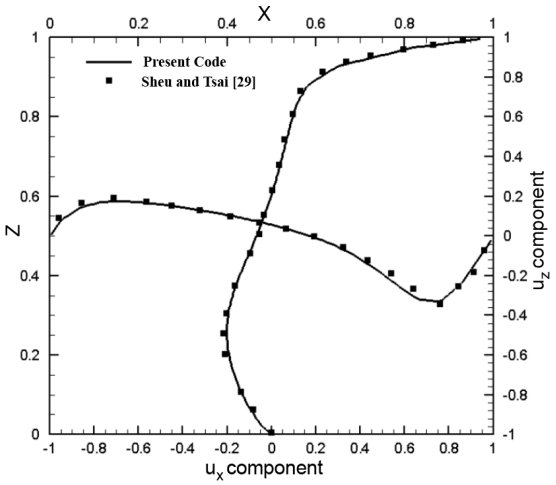

Figure 4: 3D-Lid driven velocity component (u_x) variation with respect to the height of lid (Z) and velocity component (u_Z) variation with respect to width of lid (X) at the plane of symmetry Y=0, and compared these with the well know data available in literature[29] at Re = 400.

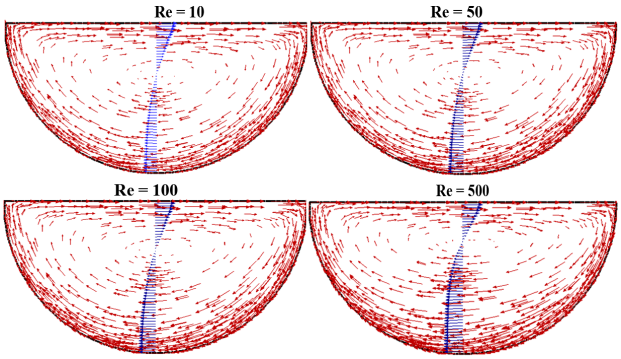

Figure 5: u_x and u_y components define the velocity vectors (red color); u_x velocity profile is also shown with respect to the vertical coordinate at X=0 in the frontal plane (Z=0) of the drop whose contact angle is 90° and Pr = 5.8.

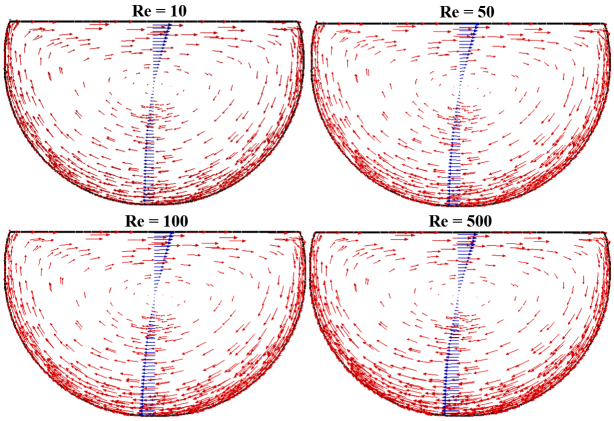

Figure 6: u_x and u_y components define the velocity vectors (red color); u_x velocity profile is shown with respect to the vertical coordinate at X=0 in the frontal plane (Z=0) of the drop whose contact angle is 105° and Pr = 5.8.

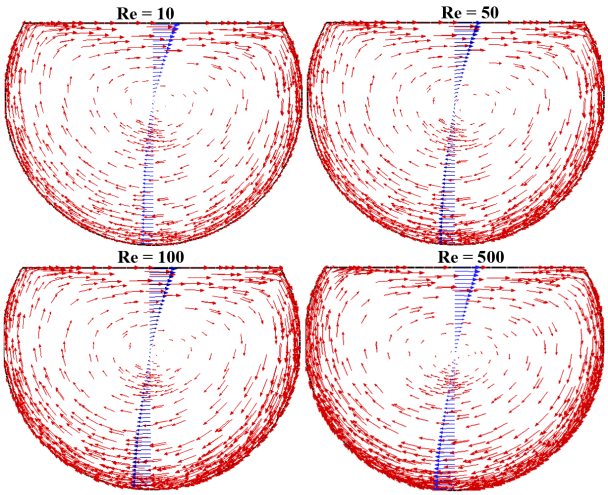

Figure 7: u_x and u_y components define the velocity vectors; u_x profile is shown with respect to the vertical coordinate at X=0 for a drop whose contact angle is 120° and Pr = 5.8.

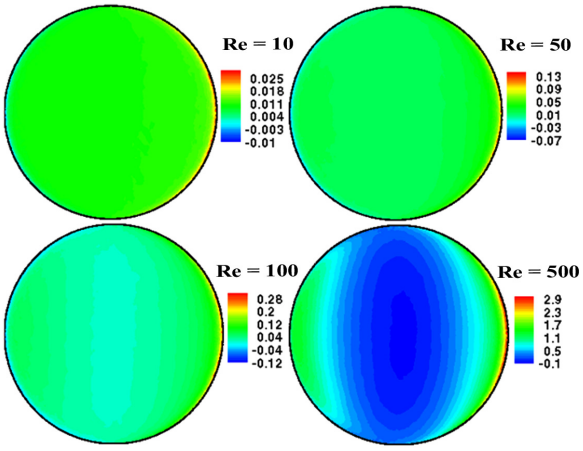

Figure 8: Wall pressure distribution for a drop of contact angle 90° at various Re and Pr = 5.8.

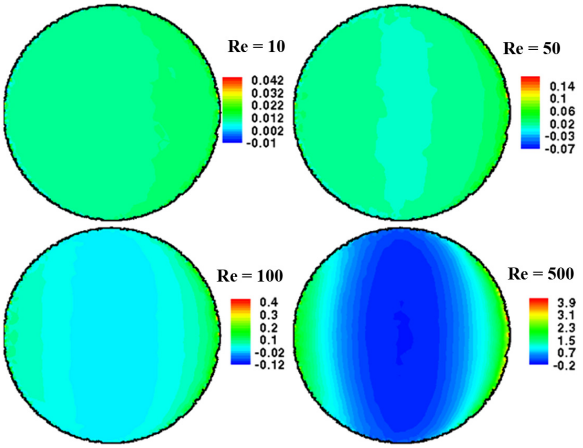

Figure 9: Wall pressure distribution for a drop of contact angle 105° at various Re and Pr = 5.8.

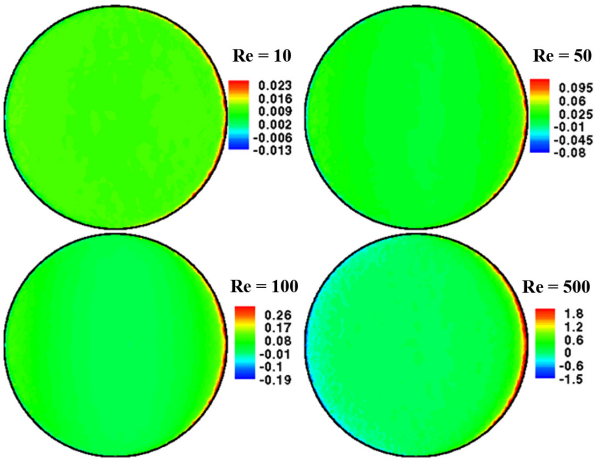

Figure 10: Wall pressure distribution for a drop of contact angle 120° at various Re and Pr = 5.8.

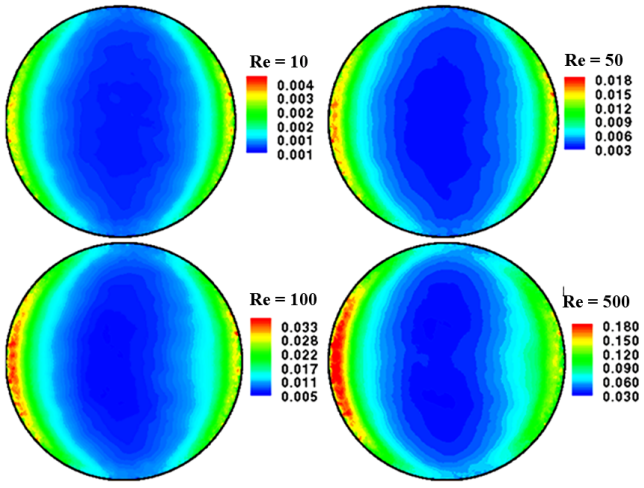

Figure 11: Wall shear stress distribution for a drop of contact angle 90° at various Re and Pr = 5.8.

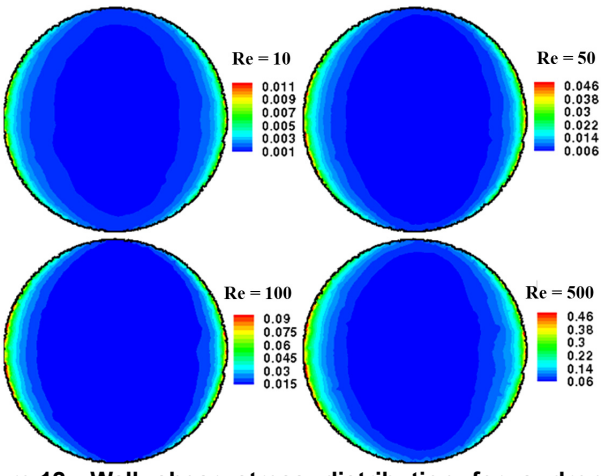

Figure 12: Wall shear stress distribution for a drop of contact angle 105° at various Re and Pr = 5.8.

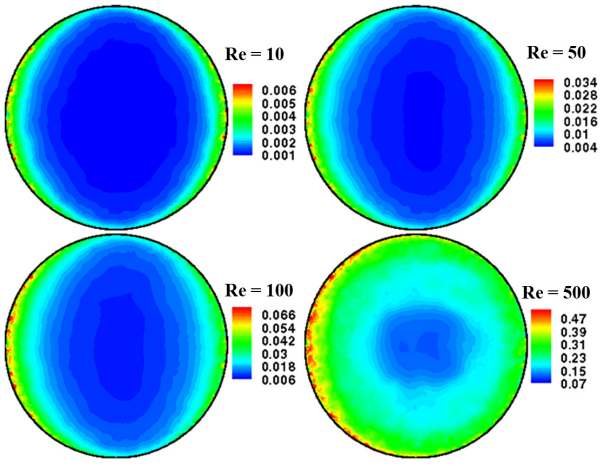

Figure 13: Wall shear stress distribution for a drop of contact angle 120° at various Re and Pr = 5.8.

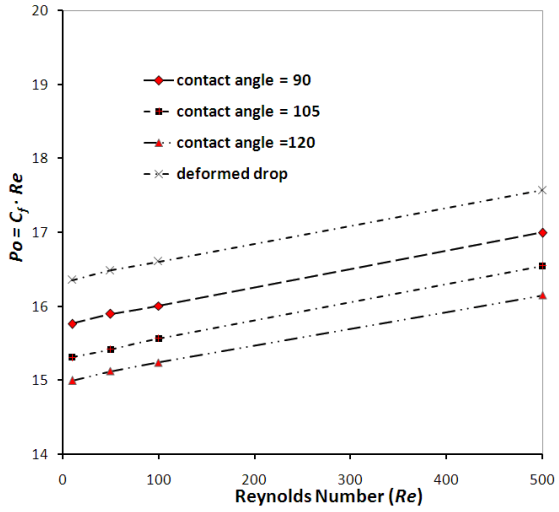

Figure 14: Poiseuille number (Po) = (C_f × Re) versus Re at Pr = 5.8 for various contact angles and deformed drop sliding underneath an inclined surface.

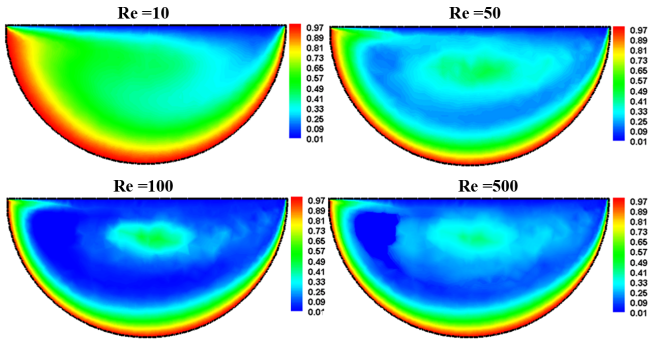

Figure 15: Non-dimensional temperature contours in the frontal plane (Z=0) of the drop of contact angle 105° for various Re and Pr = 5.8. The highest temperature is at the free surface (= 1) and the lowest temperature at the wall is (= 0).

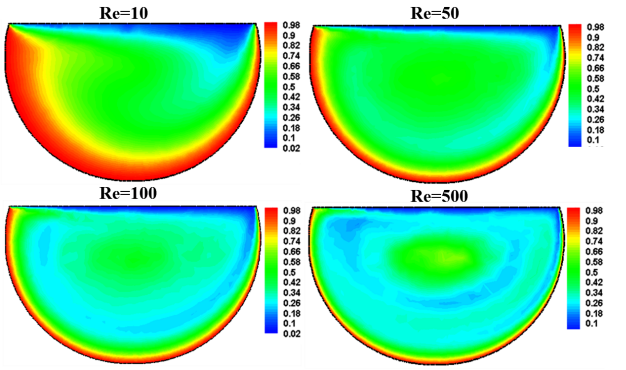

Figure 16: Non-dimensional temperature contours in the frontal plane (Z=0) of the drop of contact angle 105° for various Re and Pr = 5.8. The highest temperature is at the free surface (= 1) and the lowest temperature at the wall is (= 0).

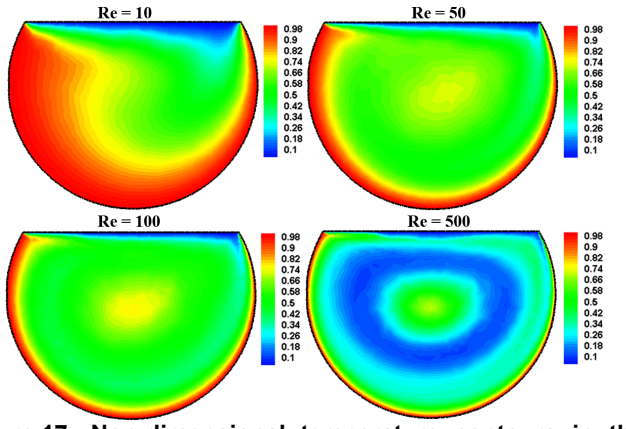

Figure 17: Non-dimensional temperature contours in the frontal plane (Z=0) of the drop of contact angle 120° for various Re and Pr = 5.8. The highest temperature is at the free surface (= 1) and the lowest temperature at the wall is (= 0).

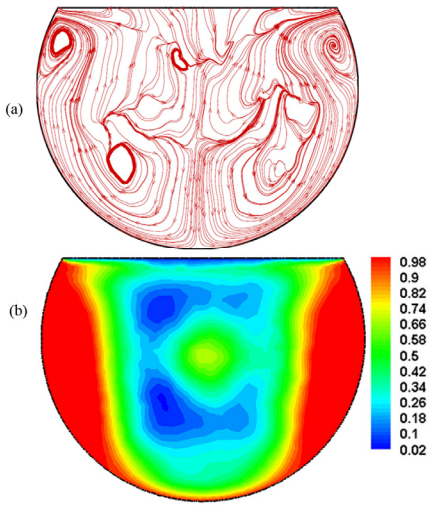

Figure18: (a) Streamlines and (b) temperature distribution at the X=0 plane for a drop of contact angle 120° at a Pr = 5.8 and Re = 500.

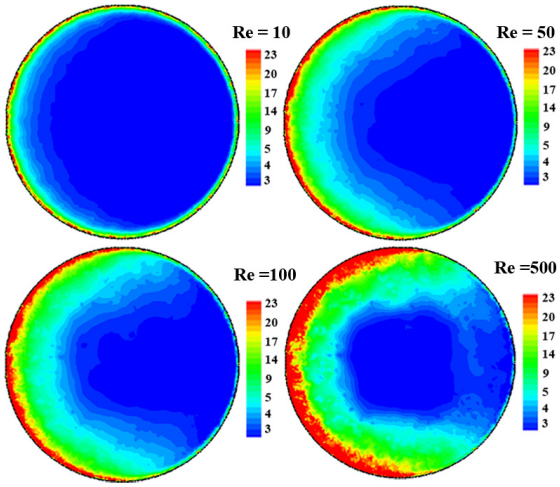

Figure 19: Nusselt number variation for a drop of contact angle 90° at various Re and Pr = 5.8.

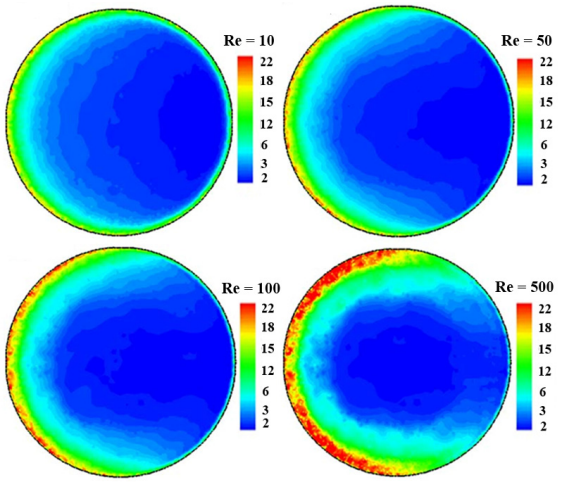

Figure 20: Nusselt number variation for a drop of contact angle 105° at various Re and Pr = 5.8.

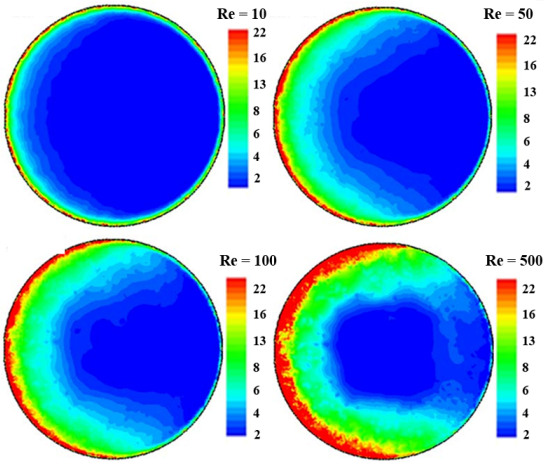

Figure 21: Nusselt number variation for a drop of contact angle 120° at various Re and Pr = 5.8.

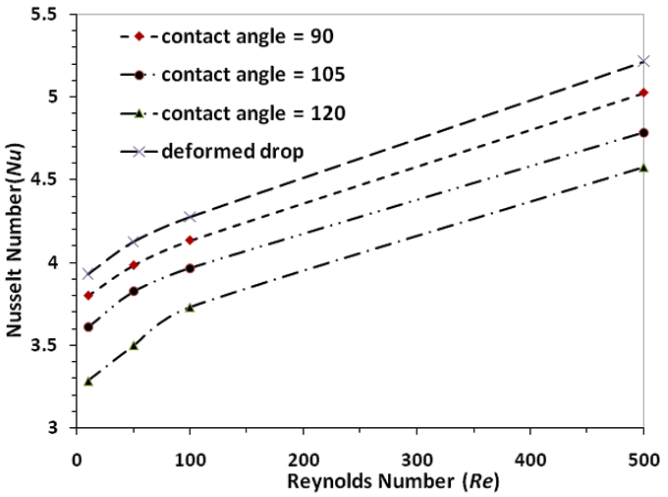

Figure 22: Nusselt number (Nu) versus Reynolds number (Re) at Prandtl number (Pr) = 5.8 for various contact angles and a deformed drop sliding underneath an inclined surface.

CONCLUSIONS

The present three dimensional numerical investigation reports fluid flow and temperature distribution inside a pendant liquid drop sliding on an inclined surface at a Prandtl number of 5.8 and various Reynolds numbers. The shape of the drop is defined by its contact angle. An attempt has been made to correlate the effective average shear stress, i.e. Poiseuille number and the net heat transfer, i.e. Nusselt number, at the droplet base, with respect to the drop Reynolds number and its shape. Such information is vital for estimating leaching rates of droplets growing and sliding on a substrate during dropwise condensation. Estimation of the leaching rates is important in many engineering applications, for example (a) estimation of life cycle of a heat exchanger textured by promoter layers and (b) estimation of substrate life on which heavy liquid metals are being deposited under closed vacuum conditions. If the ensemble droplet population under dynamic dropwise condensation process is independently known either by experiments or by simulation, the relations proposed in this work for single drops can be used to find the effective shear stress and heat transfer coefficient on the entire physically/ chemically textured condensing surface.

ACKNOWLEDGMENTS

Financial assistance provided by the Board of Research in Nuclear Sciences, Mumbai (India) is gratefully acknowledged (BRNS/ME/20050106).

REFERENCES

[1] Leach, R. N., Stevens F., Langford, S. C., and Dickinson, J. T., 2006, "Dropwise Condensation: Experiments and Simulations of Nucleation and Growth of Water Drops in a Cooling System," Langmuir, 22, pp. 8864-8872.

[2] Briscoe, B. J., and Williams, D. R. and Galvin K. P., 2005, "Condensation on Hydrosol Modified Poly-ethylene," Colloids and Surfaces A: Physicochem. Eng. Aspects, 264, pp. 101-105.

[3] Vemuri, S., and Kim, K. J., 2006, "An Experimental and Theoretical Study on the Concept of Dropwise Condensation," Int. J. Heat Mass transfer, 49, pp. 649-857.

[4] Briscoe, B. J., and Galvin, K. P., 1991, "The Sliding of Sessile and Pendent Droplets-The Critical Condition," J. Colloid and Interface Sci., 52, pp. 219-229.

[5] Battoo, N. K., Sikarwar, B. S., Khandekar, S., and Muralidhar K., 2010, "Mathematical Simulation of Dropwise Condensation Exposed to Vapor Flux," Proc. 9th Int. ISHMT - ASME Heat Mass Trans. Conf. Mumbai, India, 346, pp. 1330-1336.

[6] Sikarwar, B. S., Muralidhar, K., and Khandekar, S., 2010, "Flow and Heat Transfer in a Pendant Liquid Drop Sliding on an Inclined Plane," Proc. 9th Int. ISHMT-ASME Heat Mass Trans. Conf., Mumbai, India, 345, pp. 1322-1329.

[7] Furmidge, C. G., 1962, "The Sliding Drop on Solid Surfaces and a Theory for Spray Retention," J. Colloid Sci., 17, pp. 309-324.

[8] Dussan, E. B., 1985, "On the Ability of Drops or Bubbles to Stick to Non- horizontal Surface of Solids," J. Fluid Mech., 151, pp. 1-20.

[9] Extrand, C. W., and Kumara, Y., 1995, "Liquid Drop on an Inclined Plane: the Relation between Contact Angles, Drop Shape and Retentive force," J. Colloid and Interface Sci., 170, pp. 515-521.

[10] Sadhal, S. S., 1997, "Transport Phenomena with Drops and Bubbles", Mechanical Engineering Series, Springer New York, NY, pp. 218-230.

[11] Elsherbine, A. I., and Jacobi, A. M., 2004, "Liquid Drops on Vertical and Inclined Surfaces I: An Experimental Study of Drop Geometry," J. Colloid and Interface Sci., 273, pp. 556-565.

[12] Elsherbine, A. I., and Jacobi, A. M., 2004, "Liquid Drops on Vertical and Inclined Surfaces II. An Experimental Study of Drop Geometry," J. Colloid and Interface Sci., 273, pp. 566-575.

[13] Elsherbine, A. I., and Jacobi, A. M., 2006, "Retention Forces and Contact Angles for Critical Liquid Drops on Non-horizontal Surfaces," J. Colloid and Interface Sci., 299, pp. 841-849.

[14] Ho-Young Kim, Lee, H., and Kang, B. H., 2002, "Sliding of Drops Down an Inclined Solid Surface," J. Colloid Sci., 247, pp. 372-382.

[15] Huang, H., Liang, D., and Wetton, B., 2004, "Compotation of a Moving Drop/Bubble on a Solid Surface using a Front-Tracking Method," Comm. Math. Sci., 2, pp. 535-552.

[16] Gao, L., and McCarthy, T. J., 2006, "Contact Angle Hysteresis Explained," Langmuir, 22, pp. 6234-6237.

[17] Suzuki, S., Nakajima, A., Sakai, M., Song, J., Yoshida, N., Kameshima, Y., and Okada, K, 2006, "Sliding Acceleration of Water Droplets on a Surface Coated with Fluoroalkysline and Octadecyltrimethoxysilane," Surface Sci., 600, pp. 2214-2219.

[18] Sakai, M., Song, J., Yoshida, N., Suzuki, S., Kameshima Y. and Nakajima, A., 2006, "Direct Observation on Internal Fluidity in a Water Droplet during Sliding on Hydrophobic Surfaces," Langmuir, 22, pp. 4906-4909.

[19] Annapragada, S. R., Garimella V. S., and Murthy Y. J., 2010, "Experimental Characterization of Droplet Motion on Inclined Hydrophobic Surfaces," Proc. 9th Int. ISHMT-ASME Heat Mass Trans. Conf., Mumbai, India, 343, pp.1298-1302.

[20] Grand, N. L., Daerr, A. and Limit, L., 2005, "Shape and Motion of Drops Sliding Down an Inclined Plane," J. Fluid Mech., 541, pp. 293-315.

[21] Yoshida, N., Abe, Y., Shigeta, H., Nakajima, A., Ohsaki, K., and Watanable, T., 2006, "Sliding Behavior of Droplet on Flat Polymer Surface," J. American Chemical Society, 128, pp.743-747.

[22] Denial, S., Chaudhury, M. K., and Chen, J. C., 2001, "Fast Drop Movements Resulting from the Phase-Change on a Gradient Surface," Science, 291, pp. 633-636.

[23] Sakai, M. and Hashimoto, A., 2007, "Image Analysis System for Evaluating Sliding Behavior of a Liquid Droplet on a Hydrophobic Surface," Rev. of Scientific Instruments, 78, pp. 045105-045109.

[24] Suzuki, S., Nakajima, A., Sakai, M., Song, J., Yoshida, N., Kameshima, Y., and Okada, K, 2008, "Slipping and Rolling Ratio of Sliding Acceleration for a Water Droplet Sliding on Fluoroalkylsilane Coating of Different Roughness," Chemistry Letters, 37 pp. 58-59.

[25] Das, A. K., and Das, P. K., 2009, "Simulation of Drop Movement over an Inclined Surface using Smoothed Particle Hydrodynamics," Langmuir, 25, pp.11459-11466.

[26] Barth, T. J., and Jespersen, D. C., 1989, "The Design and Application of Upwind Schemes on Unstructured Meshes," AIAA, 89, pp. 0366.

[27] Frink, N. T., Paresh, P., and Shahyar, P., 1991, "A Fast Upwind Solver for the Euler Equations on Three Dimensional Unstructured Meshes," AIAA, 91, pp. 0102.

[28] Date, A. W., 2005, "Solution of Transport Equations on Unstructured Meshes with Cell Centered Collocated Variables. Part I: Discretization," Int. J. Heat Mass Transfer, 48, pp. 1117-1127.

[29] Sheu, T. W. H., and Tsai, A. M., 2002, "Flow Topology in a Steady Three-Dimensional Lid-Driven Cavity," Computers and Fluids, 31, pp. 911-934.

[30] Bharadvaj, B. K., Mabon, R. F., and Giddens, D. P., 1982, "Steady Flow in a Model of the Human Carotid Bifurcation - II: Laser-Doppler Anemometer Measurement," J. Bio-Mech., 15, pp. 363-378.

[31] Schwartz, M., and Tejada, S. B., 1972, "Studies of Dynamic Contact Angle on Solids," J. Colloid Interface Sci., 38, pp.359-375.

[32] Dussan, E. B., 1979, "On the Spreading of Liquid on Solid Surfaces: Static and Dynamic Contact Lines," Ann. Rev. Fluid Mech., 11, pp. 371-400.

